Simulation of Microstructural Texture Evolution in High Speed Machining of Ti-6Al-4V alloy

Xin Zhong [1, 2, a], Jun Zhao [1, 2, b *]

[1] Key Laboratory of High Efficiency and Clean Mechanical Manufacture of MOE, School of Mechanical Engineering, Shandong University, Jinan 250061, P.R. China
[2] National Demonstration Center for Experimental Mechanical Engineering Education (Shandong University), Jinan 250061, P.R. China
[a] zx126cn@126.com, [b] zhaojun@sdu.edu.cn

Keywords: Microstructural texture, Microhardness, FEM simulation, Ti-6Al-4V alloy

Abstract. This paper aims to investigate the microstructural texture evolution and microhardness of machined surface layer in high speed machining of Ti-6Al-4V alloy. Firstly, a FEM model was established to simulate the cutting process and the model was verified by cutting forces and chip morphologies obtained in high speed milling of Ti-6Al-4V alloy. Secondly, the microstructural texture of machined surface layer was simulated using the viscoplastic self-consistent (VPSC) program and the results were expressed by pole figures and orientation distribution function (ODF) diagrams using MATLAB. Finally, the microhardnesses of the cross section surface (perpendicular to the cutting speed direction) and the longitudinal section surface (parallel to the cutting speed direction) of the workpiece were measured and analyzed. The simulation results revealed that four typical shear textures (i.e. Y, C1, C2 and B fiber textures) were obtained on the machined surfaces. In addition, the microhardnesses of the cross section surface and the longitudinal section surface at the same depth below the machined surface were found to be different, demonstrating the formation of microstructural textures on the machined surfaces in high speed milling of Ti-6Al-4V alloy.

Introduction

As a two-phase titanium alloy (α phase and β phase), Ti-6Al-4V has been widely applied in various industries, especially in aerospace industry, due to its excellent mechanical properties, corrosion resistance and high strength-to-weight ratio, etc [1]. However these superior properties make Ti-6Al-4V alloy a typical difficult-to-machine material. At present, the researches on titanium alloy machining mainly concentrate on machined surface roughness, work hardening, chip formation mechanisms, cutting temperature, cutting force, fatigue strength of machined parts, etc [2-4]. There are relatively few studies on crystal orientation (texture) in machining of titanium alloy.

A crystal plasticity behavior law is always taken into account in the FEM simulation of large deformations and crystal orientations evolution of titanium alloy. And the crystal plasticity model is usually strain rate and temperature sensitive in describing the large plastic deformation behavior of polycrystalline material [5, 6]. Ayed et al. [7] utilized the crystal plasticity theory in the simulation of chip formation, phase transformation ($\alpha \rightarrow \beta$), texture evolution and cutting forces in the orthogonal micro-cutting process of titanium alloy. In our previous works [8, 9], the machined surface texture when machining titanium alloy was simulated through the variation history of shear strain and strain rate based on the perspective of plastic deformation of the machined surface layer, and typical cylinder texture and shear texture were detected in the pole figures and orientation distribution function (ODF) diagrams.

This paper mainly focuses on the study of microstructural texture evolution in the high speed orthogonal milling process of Ti-6Al-4V, and the microhardnesses of the cross section surface (perpendicular to the cutting speed direction) and the longitudinal section surface (parallel to

the cutting speed direction) of the workpiece are measured and analyzed to support the formation of textures on the machined surface of Ti-6Al-4V alloy.

Experimental Details

High speed orthogonal milling experiments were conducted using a rectangular block of Ti-6Al-4V alloy with dimensions of 100mm×20mm×3mm. The experimental setup is shown in Fig. 1. The experiments were performed on DAEWOO ACE-V500 vertical machining center using coated carbide milling cutter (Insert type: LNEQ1245R04, Coating type: KC725M). All the experiments were carried out at the cutting speeds of 60, 120 and 180m/min under dry condition with a constant axial depth of cut of 3 mm and feed rate of 0.1mm/r.

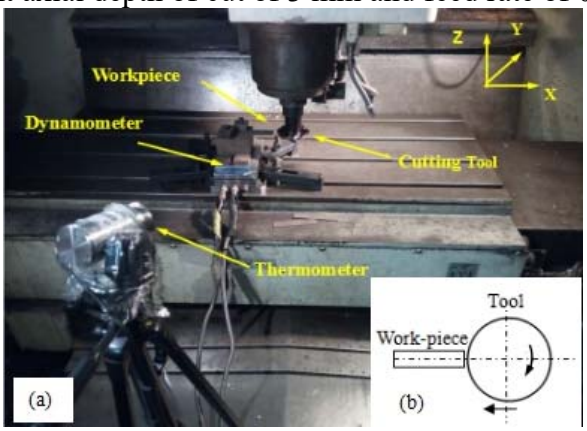

Fig. 1. Orthogonal milling experiment (a) experimental setup, (b) schematic of orthogonal milling

FE Simulation Model of Cutting

A two-dimensional orthogonal cutting model coupled with thermo-mechanical analysis of Ti-6Al-4V alloy was established using ABAQUS/Explicit. The tool and the workpiece were meshed with CPE4RT elements. The established model is shown in Fig. 2.

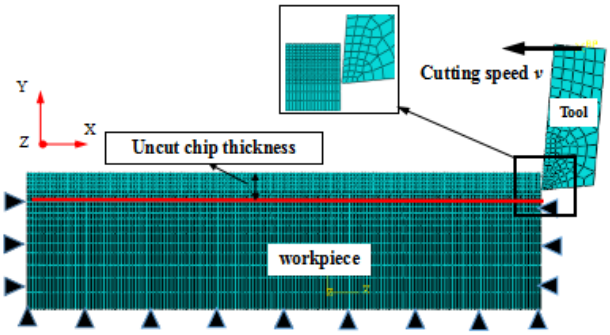

Fig. 2. Two dimensional schematic of finite element model for orthogonal cutting

The simulation adopted Johnson-Cook constitutive model to describe the relationship among flow stress, strain rate and temperature. The J-C model describes the severe plastic deformation considering the effect of strain hardening and thermal softening, which is expressed in Eq. (1).

$$\sigma_{eq} = \left(A + B\varepsilon^{n}\right)\left[1 + C\ln\left(\frac{\dot{\varepsilon}}{\dot{\varepsilon}_0}\right)\right]\left[1 - \left(\frac{T - T_0}{T_{melt} - T_0}\right)^{m}\right] \quad (1)$$

where σ_{eq} is the equivalent flow stress, ε is the equivalent plastic strain, $\dot{\varepsilon}$ is the equivalent strain rate and $\dot{\varepsilon}_0$ is the reference strain rate, T_{melt} and T_0 are melting temperature of Ti-6Al-

4V alloy and room temperature respectively. The parameters A, B, C, n and m are the initial yield stress, the hardening modulus, the strain rate dependency coefficient, the strain hardening coefficient and the thermal softening coefficient respectively, whose values are A=782.7MPa, B=498.4MPa, C=0.028, n=0.28 and m=1.0 [10] respectively.

Validation of the FE-based Cutting Simulation

The established FE-based cutting simulation model was verified by comparing the experimental and simulated principal cutting forces and chip morphologies which were obtained under cutting speeds of 60, 120, 180m/min and a constant feed rate of 0.1mm/r.

Fig. 3 gives the comparison between experimental and simulated principal cutting forces. The results show that both the experimental and simulated principal cutting forces decrease with the increase of speed, and experimental values of the principal cutting force are slightly larger than the simulated values and the errors are less than 10%. This is mainly because the cutting simulation simplifies the actual experimental conditions, without considering the vibration of machine tool and other factors.

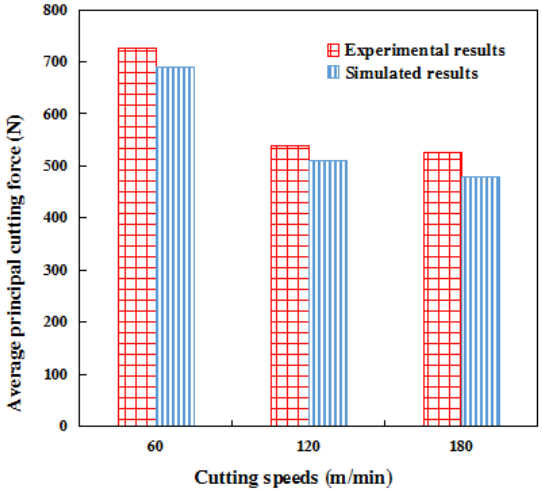

Fig. 3. Comparison between experimental and simulated principal cutting forces (f=0.1mm/r)

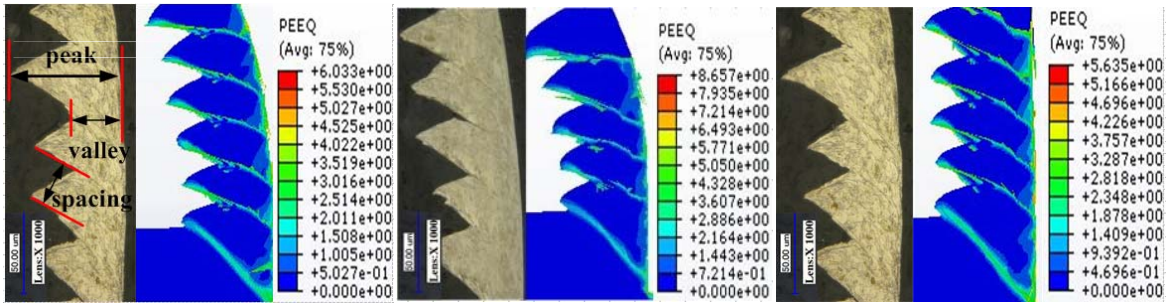

(a) v=60m/min (b) v=120m/min (c) v=180m/min

Fig. 4. Comparison between experimental and simulated chip morphologies (f=0.1mm/r)

Fig.4 shows the comparison between experimental and simulated chip morphologies under different cutting speeds. To verify the reliability of the FE model, five serrations' morphologies (chip characteristics: peak, valley, spacing) of both experimental and simulated chips were measured. The comparative results are shown in Table 1. Comparison shows that a good agreement can be detected between the experimental and simulated chip morphologies, and all the relative errors are less than 12%. Therefore, the FE-based cutting model is relatively reliable.

Table 1 Comparison between experimental and simulated chip morphology characteristics (f=0.1mm/r)

Cutting speeds		Peak (μm)	Valley (μm)	Spacing (μm)
v=60m/min	Experimental values	136	65	74
	Simulated values	127(-6.6%)	71(9.2%)	66(-10.8%)
v=120m/min	Experimental values	139	63	72
	Simulated values	133(-4.35%)	67(6.3%)	64(-11.1%)
v=180m/min	Experimental values	134	64	61
	Simulated values	124(-7.4%)	71(10.9%)	54(-11.4%)

Simulation of Microstructural Texture Evolution

The simulation results of plastic strains of machined surface in various directions after cutting showed that the shear strain γ_{xy} was the main plastic strain when compared with the very small longitudinal plastic strain ε_{xx} and transverse plastic strain ε_{yy}. Thus, the variation of plastic shear strain and strain rate with time at three points on the machined surface were extracted respectively from the simulation under different cutting conditions.

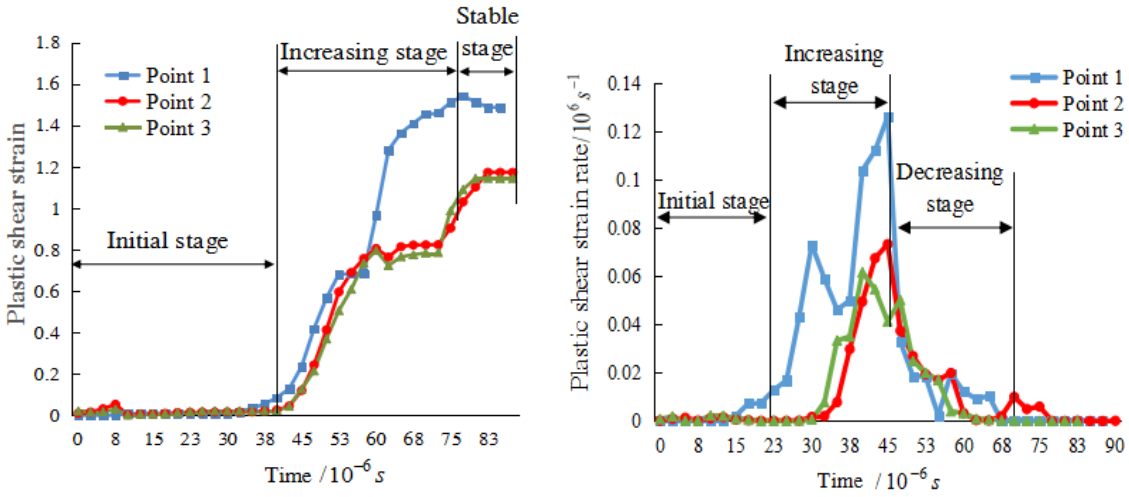

(a) Plastic shear strain (b) Strain rate

Fig. 5. Variation of plastic shear strain and strain rate versus time (v=120m/min, f=0.1mm/r)

Fig. 5 gives the variation of the plastic shear strain and strain rate with time under v=120m/min and f=0.1mm/r. All the data obtained were imported into the viscoplastic self-consistent (VPSC) program to simulate the texture of machined surface of Ti-6Al-4V, and the results were expressed by the pole figures and orientation distribution function (ODF) diagrams. Fig. 6 shows the (0001), (01 $\bar{1}$ 0), (11 $\bar{2}$ 2) pole figures and ODF diagrams of the textures for the machined surface of Ti-6Al-4V under the cutting condition of v=120m/min and f=0.1mm/r.

Results of texture simulation reveal that typical shear textures ({01 $\bar{1}$ 0}, θ=90°) are formed along the direction of cutting speed (X direction) on the machined surface of Ti-6Al-4V alloy, mainly including Y fiber texture (0°, 30°, 0~60°), C1 fiber texture (60°, 90°, 0~60°), C2 fiber texture (120°, 90°, 0~60°) and B fiber texture (0°, 90°, 0~60°). Simulation results under different cutting speeds indicate that the orientation density of texture decreases with the increase in cutting speed.

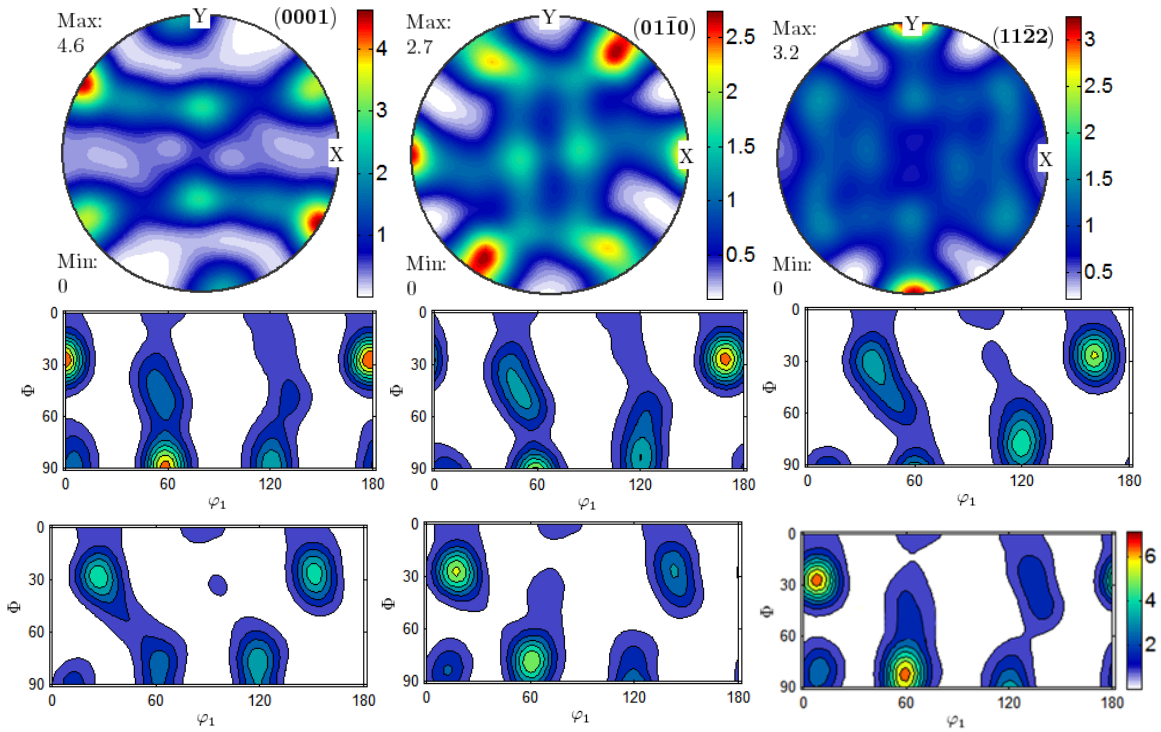

Fig. 6. Pole figures and ODF diagrams of the textures (v=120m/min, f=0.1mm/r)

Study of Microhardness in Different Directions

In order to demonstrate the texture-induced mechanical property anisotropy of the machined surface layer, the microhardnesses of the cross section surface (perpendicular to the cutting speed direction) and the longitudinal section surface (parallel to the cutting speed direction) of the workpiece were measured by using the FM 800 Microhardness tester. The schematic diagram of microhardness measurement is shown in Fig. 7.

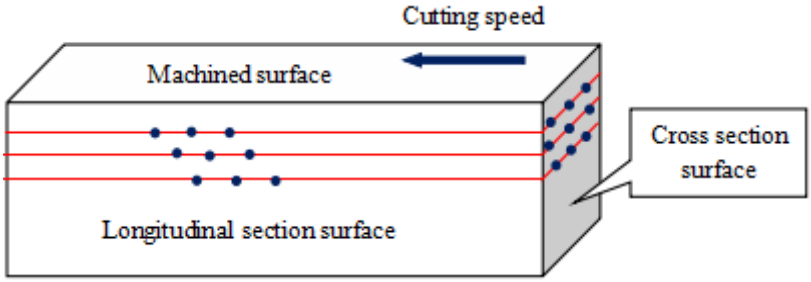

Fig. 7. Schematic diagram of microhardness measurement

Fig. 8a gives the sampling points of microhardness on the longitudinal section surface. The microhardness results of the cross section surface and the longitudinal section surface under the cutting condition of v=120m/min and f=0.1mm/r are shown in Fig. 8b. The results reveal that the microhardnesses of the two surfaces share the same trend on the whole. With the increase in distance from the machined surface, the microhardness decreases sharply at first and then increases slowly to the hardness of the unaltered bulk material, with a softened layer detected obviously at a distance of about 7~12μm from the machined surface. At the same depth below the machined surface, the microhardness of the cross section surface is slightly lower than that of the longitudinal section surface. Similar patterns of microhardness distributions are found for other cutting conditions. The formation of shear textures on the machined surface is considered to be responsible for the difference in microhardness of different surfaces.

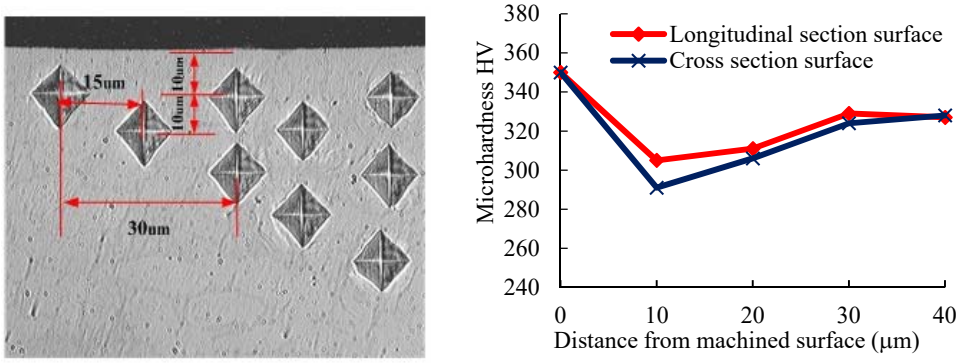

Fig. 8. (a) Sampling points of microhardness, (b) Measurement results of microhardness (v=120m/min, f=0.1mm/r)

Summary

The microstructural textures on the machined surface of Ti-6Al-4V alloy were simulated and analyzed using VPSC program based on the variation of plastic shear strain and strain rate. The results indicated that shear textures (Y, C1, C2, and B fiber textures) were formed on the machined surface and the orientation density of texture decreased with the increase in cutting speed. At the same depth below the machined surface, the microhardness of the cross section surface is slightly lower than that of the longitudinal section surface, which is a supporting evidence for the formation of textures on the machined surface of Ti-6Al-4V alloy.

Acknowledgements

This work is supported by the Key Research and Development Program of Shandong Province (2018GGX103043) and Taishan Scholars Program of Shandong Province.

References

[1] E.O. Ezugwu, Z.M. Wang, Titanium alloys and their machinability - a review, J. Mater. Process. Tech. 68 (1997) 262-274.
[2] C.H. Che-Haron, A. Jawaid, The effect of machining on surface integrity of titanium alloy Ti-6%Al-4%V, J. Mater. Process. Tech. 166 (2005) 188-192.
[3] M.-B. Mhamdi, M. Boujelbene, E. Bayraktar, et al., Surface integrity of titanium alloy Ti-6Al-4V in ball end milling, Physics Procedia 25 (2012) 355-362.
[4] C.-F. Wyen, K. Wegener, Influence of cutting edge radius on cutting forces in machining titanium, CIRP Annals - Manufacturing Technology 59 (2010) 93-96.
[5] M. Ardeljan, I.J. Beyerlein, B.A. McWilliams, et al., Strain rate and temperature sensitive multi-level crystal plasticity model for large plastic deformation behavior: application to AZ31 magnesium alloy, Int. J. Plasticity 83 (2016) 90-109.
[6] Z. Liu, P. Li, L. Xiong, et al., High-temperature tensile deformation behavior and microstructure evolution of Ti55 titanium alloy, Mater. Sci. Eng. A 680 (2017) 259-269.
[7] Y. Ayed, C. Robert, G. Germain, et al., Orthogonal micro-cutting modeling of the Ti17 titanium alloy using the crystal plasticity theory, Finite Elem. Anal. Des. 137 (2017) 43-55.
[8] A. Li, J. Pang, J. Zhao, et al., FEM-simulation of machining induced surface plastic deformation and microstructural texture evolution of Ti-6Al-4V alloy, Int. J. Mech. Sci. 123 (2017) 214-223.
[9] J.M. Pang, J. Zhao, A.H. Li, et al., Crystical plasticity and analysis of machined surface of titanium alloy, Mach. Des. Manuf. 4 (2018) 159-161. (In Chinese)
[10] W.S. Lee, C.F. Lin, High-temperature deformation behavior of Ti6Al4V alloy evaluated by high strain-rate compression tests, J. Mater. Process. Tech. 75 (1998) 127-136.